Depletion of Plasma Membrane PI4P by ORP5 Requires Hydrolysis by SAC1 in Acceptor Membranes

Colleen P. Doyle, Liz Timple and Gerald R. V. Hammond

Department of Cell Biology, University of Pittsburgh School of Medicine, Pittsburgh, PA 15261.

Correspondence: ghammond@pitt.edu

Keywords: Lipid transfer proteins; membrane contact sites; phosphoinositides; PtdIns4P.

Running title: PI4P transport by ORP5 is coupled to lipid hydrolysis

Abstract

Oxysterol binding protein (OSBP)-related proteins (ORPs) 5 and 8 have been shown to deplete the lipid phosphatidylinositol 4-phosphate (PI4P) at sites of membrane contact between the endoplasmic reticulum (ER) and plasma membrane (PM). This is believed to be caused by transport of PI4P from the PM to the ER, where PI4P is degraded by an ER-localized SAC1 phosphatase. This is proposed to power the anti-port of phosphatidylserine (PS) lipids from ER to PM, up their concentration gradient. Alternatively, ORPs have been proposed to sequester PI4P, dependent on the concentration of their alternative lipid ligand. Here, we aimed to distinguish these possibilities in living cells by orthogonal targeting of ORP5 to PM-mitochondrial contact sites. We demonstrate that ORP5 is unable to deplete PM PI4P or accumulate the lipid in mitochondrial outer membranes when acting alone, ruling out both lipid transport and sequestration models. However, when combined with orthogonal targeting of SAC1 to the mitochondrial outer membrane, ORP5 facilitates depletion of PM PI4P when targeted to PM-mitochondria contact sites. We conclude that PI4P depletion from the PM by ORP5 requires transport of PI4P to the tethered organelle membrane, which must be closely coupled to PI4P hydrolysis by SAC1. The data are most compatible with a lipid transfer reaction by ORP family members.

Introduction

The exchange of lipids by non-vesicular lipid transport is a core function of membrane contact sites between organelles (Prinz et al., 2020). This process can be mediated by soluble or tethered lipid transfer proteins that bind and solubilize individual lipids, or else proteinaceous conduits that permit lipids to flow between membranes (Wong et al., 2019). However, these proteins present a thermodynamic conundrum: Lipid exchange is known to enrich specific lipids in one membrane relative to the other at the contact site, yet the proteins themselves employ what is essentially a passive transport process. In other words, how can a lipid transfer protein move a lipid up a concentration gradient?

A seminal discovery shed light on one answer to this question (Saint-Jean et al., 2011): the discovery that Osh4p, a yeast member of the ORP family, can bind to both sterols and a phosphoinositide, PI4P. It followed that ORPs could employ an anti-porter mechanism; specifically, a phosphoinositide concentration gradient is created between the trans-Golgi network (TGN) and the ER by TGN localized PI 4-kinases (PI4Ks) that generate PI4P, and the ER-localized SAC1 phosphatase that degrades it. Transport of PI4P down this gradient by Osh4p releases energy used to counter-transport sterol from the ER back to the TGN, up its gradient. Ultimately, the energy of ATP hydrolysis is coupled to sterol transport via PI4P turnover. The mechanism was subsequently demonstrated for cholesterol transport at the mammalian TGN by OSBP (Mesmin et al., 2013), and was expanded to include PS transport from ER to PM by ORP5 and ORP8 in humans (Chung et al., 2015) and the homologues Osh6p and Osh7p in yeast (Filseck et al., 2015).

An implicit assumption of this model is that SAC1 activity acts to deplete PI4P and maintain the gradient, acting downstream of PI4P transport. It follows that ablation of SAC1 activity would lead to the accumulation of PI4P in the ER, which has been observed (Cheong et al., 2010; Zewe et al., 2018). However, PI4P transport by ORP family proteins remains controversial. An alternative hypothesis posits that ORP proteins act as negative regulators of PI4P signaling by sequestering the lipid, and that this inhibition can be relieved by high local concentrations of the counter lipid such as sterol (Wang et al., 2019). Thus, the alternative lipid cargoes modulate available PI4P pools. Differentiation of these mechanisms can be difficult in cells, where both hypotheses predict decreases in accessible PI4P levels by ORPs in donor membranes like the PM or TGN.

Here, we sought to test the PI4P transfer activity of the human ORP5 protein via orthogonal targeting to different sites of membrane contact – namely between the PM and mitochondrial outer membrane. We show that under these conditions, ORP5 cannot deplete PM PI4P unless SAC1 is ectopically targeted to the mitochondrial outer membrane. The results are compatible with PI4P transport by ORP5, which must be coupled to PI4P hydrolysis to prevent re-binding of PI4P to the high affinity OSBP-related domain (ORD).

Results

ORP5 contains an N-terminal extended Pleckstrin Homology (PH) domain that interacts selectively with the PM via PI4P and PI(4,5)P_2 (Sohn et al., 2018); this is connected to the ORD lipid-transfer domain by a long region of low complexity, and is anchored to the ER by a C-terminal transmembrane helix (cartoon in **Fig. 1A**). When expressed as an mCherry-fusion, ORP5 localizes exclusively to ER-PM contact sites, co-localizing with the ER-PM contact site marker MAPPER (Chang et al., 2013) when viewed by equatorial or ventral confocal sections (**Fig. 1A**).

Previously, acute depletion of PM PI4P was demonstrated by replacing the N-terminal PH domain with the FK506 binding protein (FKBP) domain, and inducing FKBP dimerization with a PM anchored FK506 and Rapamycin Binding domain of mTor (FRB) via the addition of rapamycin. This acute restoration of ORP5 ER-PM contact site localization was presumed to induce transport of PM PI4P to the ER, where it was degraded by SAC1 (Chung et al., 2015). To facilitate orthogonal contact site formation between the PM and another organelle (thereby uncoupling ORP5 transport from degradation by ER SAC1), we instead replaced the C-terminal ER-localizing helix with FKBP, a fusion henceforth termed ORP5$^{\Delta TMD}$-FKBP (cartoon in **Fig 1B**). This generates a PM localization no longer restricted to MAPPER-labelled ER-PM contact sites (**Fig. 1B**).

We then acutely restored ORP5$^{\Delta TMD}$-FKBP localization to ER-PM contact sites by rapamycin-induced dimerization with an ER-anchored FRB domain (**Fig 1C**). Such sites formed rapidly (completing within ~5 min) when viewed by ventral confocal section. In parallel, we tracked the distribution of PI4P using the high affinity lipid biosensor EGFP-P4Mx2 (Hammond et al., 2014). As expected, we did not see accumulation of PI4P at these contact sites (see graph in **Fig. 1C**), presumably due to SAC1 activity in the ER. Rather, the fluorescence of PM PI4P seemed to decline, though this is not as obvious when viewed by confocal in such ventral focal planes.

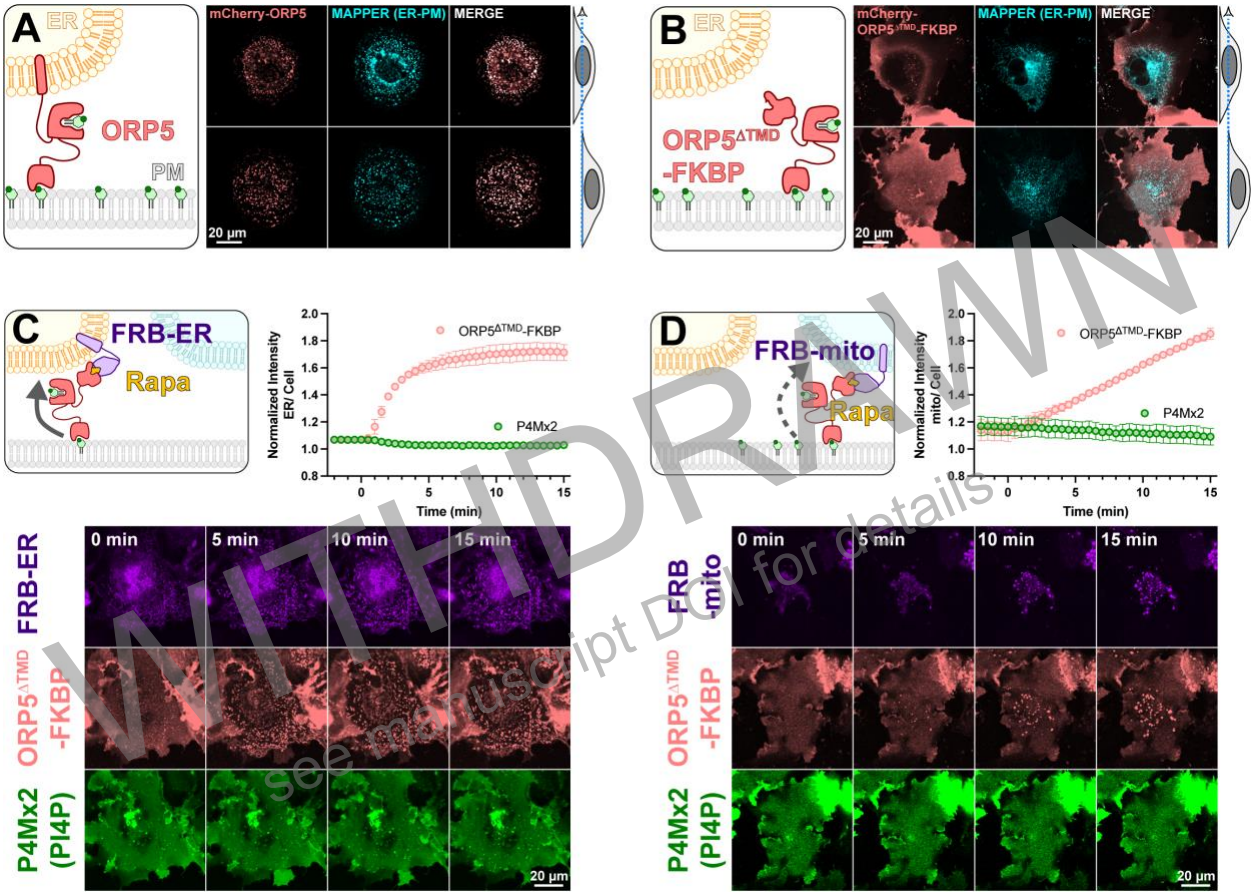

Figure 1: An engineered ORP5 ectopically targeted to PM-mitochondria contact sites fails to transfer PI4P. (**A**) mCherry-ORP5 localizes to ER-PM contact sites marked by the ER-PM contact site marker, MAPPER. Images show equatorial and ventral confocal sections of the same, representative cells. (**B**) Replacement of the ER-resident transmembrane domain (TMD) of ORP5 with FKBP leads to a de-localized PM localization, overlapping with MAPPER-labelled ER-PM contact sites, but not restricted to them. (**C**) mCherry-ORP5$^{\Delta TMD}$-FKBP can be returned to ER-PM contact sites by rapamycin-induced dimerization with an ER-localized FRB domain (iRFP-FRB-ER) though no enrichment of PI4P is seen at these induced contact sites. (**D**) mCherry-ORP5$^{\Delta TMD}$-FKBP can be targeted to ectopic mitochondria-PM contact sites by rapamycin-induced dimerization with an mitochondria-localized FRB domain (AKAP1^{N31}-FRB-iRFP), though again no enrichment of PI4P is seen at these induced contact sites. For **C & D**, images show ventral confocal sections of representative cells; the graphs show the normalized mCherry-ORP5$^{\Delta TMD}$-FKBP or P4Mx2 PI4P biosensor enrichment at ER or mitochondria contact sites, respectively. Data are grand means ± s.e. of three experiments, with 10 cells per experiment.

We next sought to test whether orthogonal targeting of ORP5$^{\Delta TMD}$-FKBP to PM-mitochondrial contact sites would cause accumulation of PI4P in the latter organelle. Rapamycin induced dimerization recruited ORP5$^{\Delta TMD}$-FKBP to bright patches marked by mitochondria outer membrane-localized FRB, albeit somewhat more slowly than it recruits to ER-localized FRB (**Fig. 1D**). However, we saw no evidence of PI4P accumulation at these PM-mitochondria contacts (**Fig. 1D**).

A number of scenarios could be envisioned that may preclude productive transfer of PM PI4P to mitochondria by ORP5$^{\Delta TMD}$-FKBP. One possibility is suggested by recent studies of the homologous yeast protein, Osh6p (Eisenreichova et al., 2021). That study reported that binding of PI4P by Osh6p is so tight that lipid transfer is actually inhibited. Hydrolysis of PI4P was required to deplete the lipid and permit PS binding in these experiments. We therefore hypothesized that SAC1 activity may in fact be required for productive release of the PI4P. To test this, we engineered SAC1 to ectopically target mitochondria. We replaced the ER-localized transmembrane domains with the mitochondrial outer membrane-targeting C-terminal 31 amino acids from Fis1 (Stojanovski et al., 2004), generating SAC1^{mito}. This construct (fused to EGFP or TagBFP2) localized well to mitochondria (**Fig. 2A**), demonstrated by its close co-localization with a mitochondrial-matrix targeted mCherry (Filippin et al., 2005).

To demonstrate activity of SAC1^{mito}, we capitalized on our recent demonstration that PI4P synthesis can be ectopically induced on the mitochondria outer membrane by recruitment of the C-terminal helical-catalytic domain of PI4KA (Zewe et al., 2020). As shown in the left hand panels of **Fig. 2B**, PI4P accumulation is readily detected with PI4P biosensor, P4M (Hammond et al., 2014). Co-expression of SAC1^{mito} under these conditions completely abolishes PI4P accumulation under these conditions (right hand panels in **Fig. 2B** and **Fig. 2C**), despite identical recruitment of the PI4K (inset in **Fig. 2C**). We did note a small decrease in baseline mitochondria associated P4M fluorescence in Sac1^{mito}-expressing cells (**Fig. 1C**), though this was not statistically significant (**Fig. 2D**). The block in PI4P synthesis induced by SAC1^{mito} was complete, showing no significant deviation from 0 when measuring the area under the curve (**Fig. 2E**). Therefore, we could reconstitute ER-like PI4P degradation on the mitochondrial outer membrane.

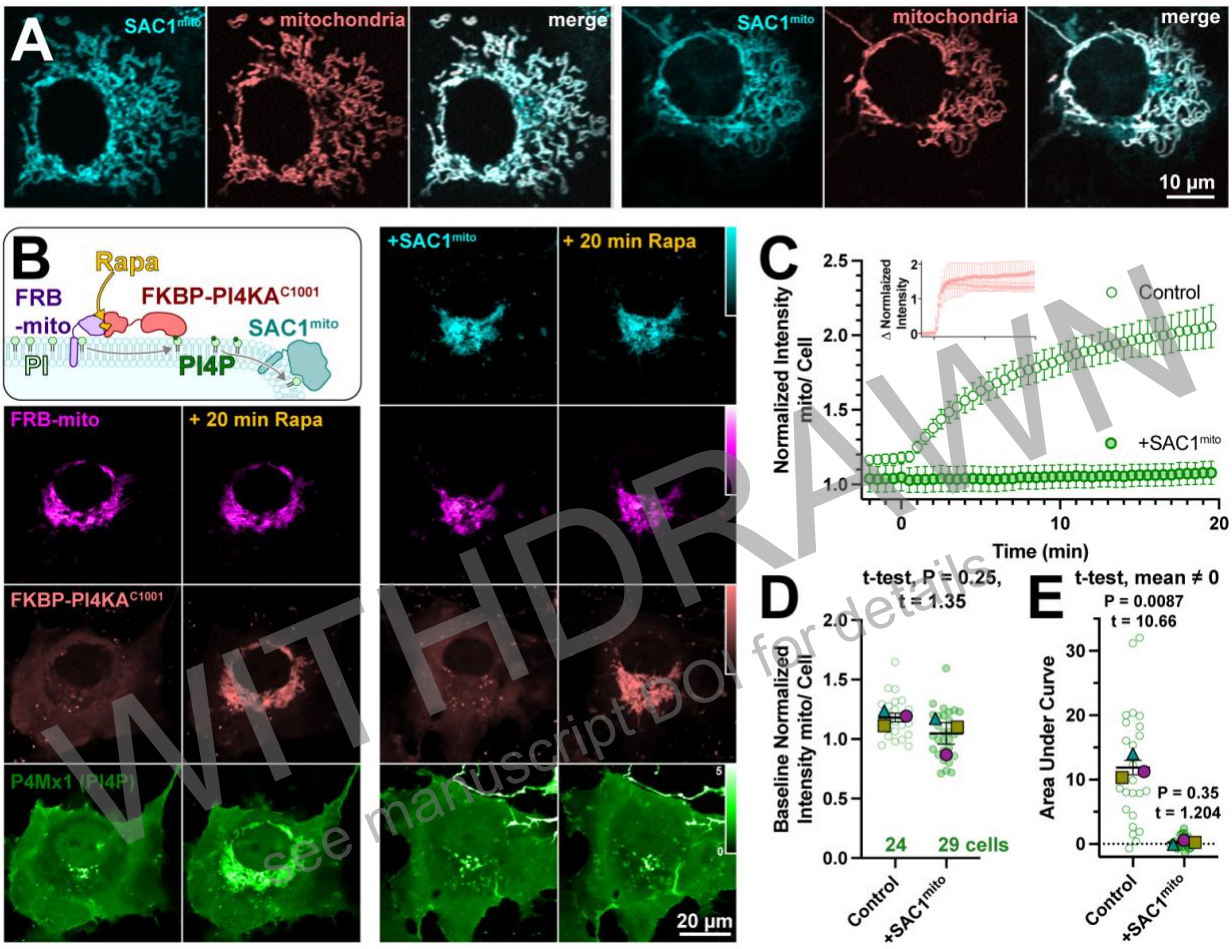

Figure 2: An engineered mitochondria-targeted SAC1 is active in cells. (**A**) SAC1^{mito} co-localizes with the mitochondrial marker, COX8A^{N29}x2-mCherry (pink). Images show representative equatorial confocal sections of two COS-7 cells. (**B**) Mitochondrial PI4P synthesis was induced by addition of rapamycin, which induces dimerization of over-expressed mCherry-FKBP-PI4K^{C1001} with iRFP-FRB-mito; this initiates ectopic PI4P synthesis on mitochondria outer membranes, detected with EGFP-P4Mx1 biosensor. The accumulation is blocked by co-expression of tagBFP2-SAC1^{mito}. Images show equatorial confocal sections of COS-7 cells before or after addition of rapamycin. P4Mx1 intensity is normalized to the average cell intensity, as quantified in B. (**C**) PI4P accumulation on mitochondria is blocked by SAC1^{mito}, despite equally efficient PI4KA^{C1001} recruitment (inset). (**D**) The slightly decreased baseline level of PI4P at mitochondria is not statistically significant by nested t-test. Smaller green points show individual cells (7-11 cells/experiment) and larger colored shapes show means of each of 3 experiments. Grand means ± s.e.m. are also indicated. (**E**) Complete reduction of mitochondrial PI4P synthesis, demonstrated by a grand mean of the area under the curve for SAC1^{mito}-expressing cells of 0.24 ± 0.20, not significantly different from 0 by t-test.

Armed with this construct, we set out to reconstitute PI4P transfer at mitochondria. For these experiments, we elected to acutely stop *de novo* PI4P synthesis in the PM using the PI4KA inhibitor GSK-A1 (Bojjireddy et al., 2014). The rationale was that without inhibition of PI4P synthesis, observing reductions in PM PI4P catalyzed by transport of PI4P out of the PM would require a rate that exceeded synthesis, which may not be possible through reduced flux at the much smaller surface area of induced PM-mitochondria contact sites, compared to ER-PM contact sites (compare **Figs. 1C** and **D**). We also imaged by Total Internal Reflection

Fluorescence Microscopy (TIRFM) to more sensitively detect changes in PM PI4P with the high affinity PI4P biosensor, P4Mx2.

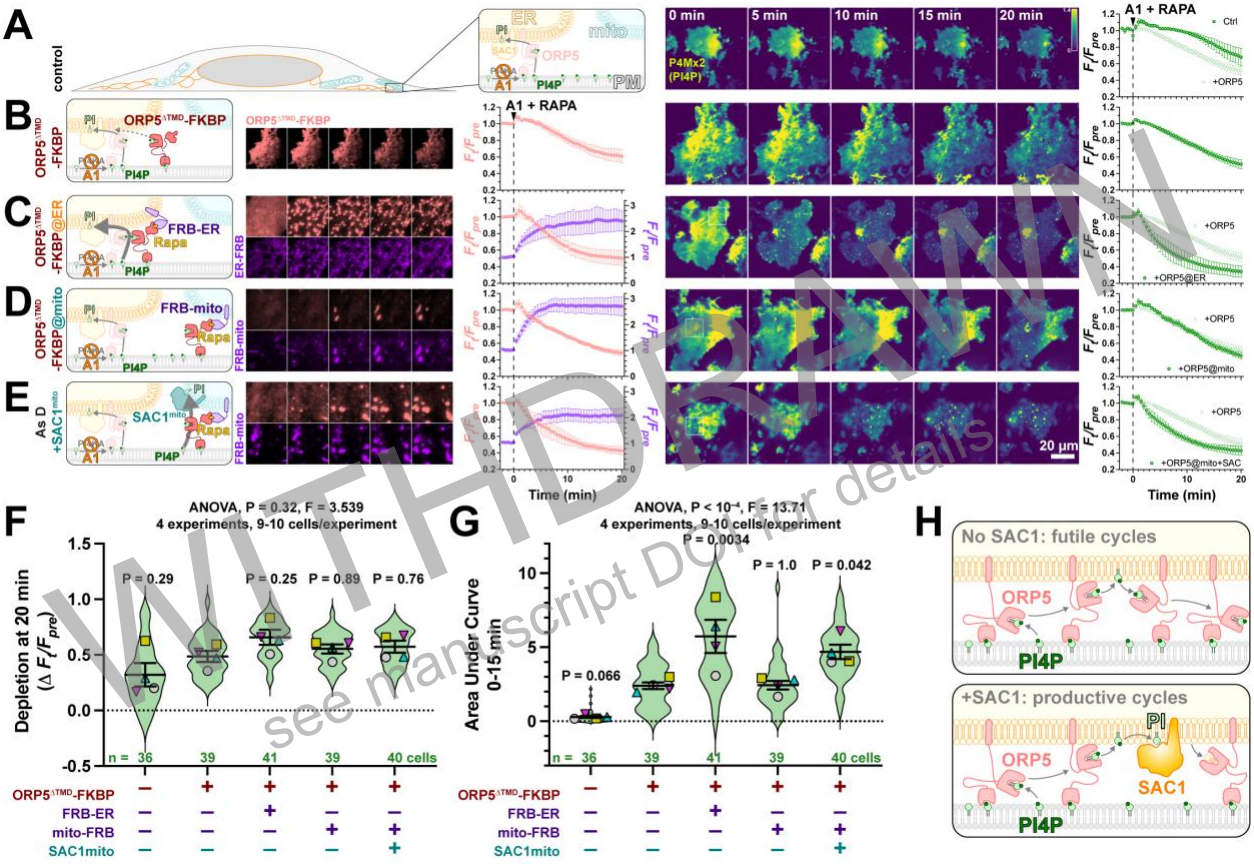

Figure 3: PI4P hydrolysis is required for productive inter-organelle PI4P transfer cycles (**A-E**) PI4P levels in COS-7 cells were measured with TIRFM using EGFP-P4Mx2 biosensors. At time 0, 1 µm rapamycin was applied to induce dimerization of any expressed FRB and FKBP proteins, along with 30 nM GSK-A1 to stop PM PI4P synthesis by PI4KA. PI4P turnover is then assessed over 20 mins. Graphs at right of images show the quantification of fluorescence intensity from color-matched channels to the left. 15 µm insets are displayed for FRB and FKBP where indicated on the PI4P images of whole cells. (**A**) In control cells, PI4P depletion is expected to occur due to transfer of PI4P to ER-localized SAC1 by endogenous ORP5, among other mechanisms. (**B**) over-expression of mCherry-ORP5$^{\Delta TMD}$-FKBP may slightly accelerate depletion, whereas recruitment of the protein using an ER-localized FRB (iRFP713-FRB-SAC1^{TMD}, **C**) causes greatly accelerated PM PI4P depletion. On the other hand, recruitment of mCherry-ORP5$^{\Delta TMD}$-FKBP to mitochondrial outer membrane localized FRB (iRFP713-FRB-Fis1^{C31}, **D**) does not accelerate PI4P depletion, unless it is co-expressed with a mitochondrial outer membrane-localized SAC1 (SAC1^{mito}, **E**). Graphs show means ± s.e. of the grand means of four experiments. Statistical analysis is presented for the total extent of depletion of PI4P at 20 mins in **F** or the rate of depletion (assessed as area under the curve during the first 15 mins) in **G**. Violin plots show the distribution of values from all cells measured across all four experiments; overlaid points show means of each experiment, and line and error bars show grand mean ± s.e. The results of a one-way nested-ANOVA are indicated, with Dunnet's post-hoc analysis comparing all values to mCherry-ORP5$^{\Delta TMD}$-FKBP alone. (**H**) Model for how SAC1 prevents futile cycles due to high-affinity binding of ORP5 ORD to PI4P.

Addition of GSK-A1 to control cells expressing P4Mx2 led to a slow, somewhat lagging decline in PI4P levels (**Fig. 3A**), consistent with previous reports (Sohn et al., 2018). Over-expression of ORP5$^{\Delta TMD}$-FKBP by itself (with no recruiting partner) appeared to increase the rate of PI4P

decline slightly (**Fig. 3B**), though neither the extent (**Fig. 3F**) nor the rate (assessed as Area Under the Curve for the first 15 min where the curves diverge, **Fig. 3G**) was significantly altered. However, when ORP5$^{\Delta TMD}$-FKBP was recruited to ER-anchored FRB, we observed greatly accelerated depletion of PM PI4P (**Figs. 3C** and **G**), though the extent was still not significantly altered (**Fig. 3F**). Thus, we could show that our ORP5 truncation retained activity. Note that when GSK-A1 was added to cells, total PM fluorescence of ORP5$^{\Delta TMD}$-FKBP declined, whether or not it was recruited to sites of membrane contact (pink curves, **Figs. 3B-E**). This is caused by depletion of PI4P, which is required for the ORP5 PH domain to bind to the PM (Chung et al., 2015; Sohn et al., 2018).

When ORP5$^{\Delta TMD}$-FKBP was recruited to PM-mitochondria contact sites, we observed no difference in the rate or extent of PI4P decline relative to the expression of the construct without recruitment (**Figs 3D, F, G**). On the other hand, when cells also expressed SAC1^{mito}, a rapid clearance of PM PI4P was observed (**Fig 3E**), similar to what we observed for ER recruitment (**Fig. 3C**). This depletion was significantly faster in terms of rate (**Fig. 3F**) but not magnitude (**Fig. 3G**). Overall, these experiments demonstrate that clearance of PM PI4P by ORP5 absolutely requires the presence of PI4P-degrading SAC1 in the acceptor membrane.

Discussion

We designed these experiments to unambiguously demonstrate PI4P transfer activity of ORP5 in living cells by orthogonal targeting to PM-mitochondria contact sites, hoping to demonstrate catalyzed transfer of PI4P lipids to the mitochondrial outer membrane. Our experiments failed in this endeavor (**Fig. 1**). However, we did demonstrate the ability of ORP5 to deplete PM PI4P after tethering to a site of membrane contact with another organelle, so long as SAC1 is present in that tethered organelle membrane.

In principle, this observation does not demonstrate lipid transfer (though it is compatible with it). Although tethering at a site of membrane contact seems to facilitate access of PI4P to SAC1, ORP5 could simply be presenting the lipid to the phosphatase, as opposed to depositing PI4P into the membrane for subsequent hydrolysis by SAC1. If ORP5 works in such a presentation mode, it is not clear to which membrane the resulting PI lipid is released: either back into the PM, or into the tethered membrane. In other words, lipid transfer is not necessarily part of the reaction.

Our results make perfect sense in the light of recent, elegant in vitro experiments with Osh6p in artificial membranes (Eisenreichova et al., 2021). Here, the ORD domain was shown to have exceptionally high affinity for PI4P, such that it actually inhibited binding and transport of the counter lipid, PS. These experiments predicted and demonstrated a requirement for PI4P hydrolysis for PS transport to occur. This high affinity suggests that the slow release (off rate) and rapid binding (on rate) of PI4P to ORD may cause rapid re-binding of released PI4P molecules at tethered membranes; lipid transfer would be effectively stalled and the ORD would be saturated with PI4P (**Fig. 3H**, upper panel). Efficient PI4P hydrolysis by SAC1 at the tethered membrane prevents this, facilitating counter lipid transport (**Fig. 3H**, lower panel). Such a mechanism will reduce the propensity of futile transfer cycles in both directions: High affinity PI4P binding over PS ensures PI4P is selectively bound, and only this lipid travels down the concentration gradient; rapid hydrolysis of PI4P in the ER ensures this favorable binding cannot happen, and so binding and transfer of the lower affinity PS occurs.

That said, high affinity PI4P binding to the ORD is also envisioned in the counter-lipid sensing model (Wang et al., 2019), where the ORP proteins effectively sequester pools of PI4P, inhibiting regulation of other effector proteins. High concentrations of counter lipids compete with PI4P binding to the ORD, releasing a pool of PI4P to activate these effectors. Could such a model operate? The approximate concentration of phosphoinositides like PI4P and $PI(4,5)P_2$ in a typical animal cell (assuming, incorrectly, they are dissolved in the volume of the cell and not on membranes) is in the order of 10 µM (McLaughlin et al., 2002). Recent proteomic data reveal the equivalent concentration of all ORP proteins in a HEK293 cell to be approximately 1.2 µM. Therefore, saturated ORPs could at most sequester ~10% of the PI4P in a cell. However, given the high degree of concentration of ORPs at specific sites of membrane contact, local sequestration of a much larger fraction of the local PI4P pool, perhaps even all of it, is plausible.

On the other hand, with such a high concertation of ORPs relative to PI4P, the slow *in vitro* transfer rates of ~30 PI4P molecules per ORP per minute (Lipp et al., 2019; Mesmin et al., 2013) could easily cause transport the entire pool of PI4P to the ER for degradation in under a minute. This is certainly faster than the time scale for depletion of any of the PI4P pools made by any of the PI4Ks (Sengupta et al., 2019; Sohn et al., 2018; Tóth et al., 2006). Therefore, lipid transfer is also certainly plausible given these constraints.

In conclusion, although our results do not provide unequivocable evidence of PI4P transport by ORP5, they do demonstrate that depletion of PM PI4P by this protein absolutely requires its

localization to a membrane contact site, and coupling to SAC1 activity in the tethered membrane compartment. These data are most consistent with a lipid transfer model.

Materials and Methods

Plasmids

The following plasmids were obtained as cited, or else generated by polymerase chain reaction and HiFi assembly (New England Biolabs) according to the manufacturer's instructions:

Plasmid	Backbone	Insert	Reference
NES-EGFP-P4Mx1	pEGFP-C1	*X.leavis* map2k1.L(32-44):EGFP:*L. pneumophila* SidM$^{546-647}$	(Zewe et al., 2018)
EGFP-P4Mx2	pEGFP-C1	EGFP:*L. pneumophila* SidM(546-647):SidM$^{546-647}$	(Hammond et al., 2014)
EGFP-MAPPER	pEGFP-C1	EGFP:MAPPER	(Chang et al., 2013)
mCherry-ORP5	pmCherry-C1	mCherry:OSBPL5(isoform a)	(Sohn et al., 2018)
mCherry-ORP5$^{\Delta TMD}$-FKBP	pmCherry-C1	mCherry:OSBPL5(isoform a)$^{1-856}$:FKBP$^{3-108}$	This study
Akap1^{N31}-FRB-iRFP	piRFP-N1	*Mus musculus* Akap1$^{1-31}$-M16L:MTOR$^{2021-2113}$:iRFP	(Zewe et al., 2020)
iRFP-FRB-ER	piRFP-C1	iRFP: MTOR$^{2021-2113}$:[GGSA]$_2$ILNSRV:SACM1L(521-587)	(Zewe et al., 2020)
COX8AN29x2-mCherry	pmCherry-N1	COX8A$^{1-29}$:mCherry	(Zewe et al., 2020)
EGFP-SAC1^{mito}	pEGFP-C1	EGFP:SACM1L$^{1-521}$:FIS1$^{122-152}$	This study
TagBFP2-SAC1^{mito}	pTagBFP2-C1	TagBFP2:SACM1L$^{1-521}$:FIS1$^{122-152}$	This study
iRFP-FRB-mito	piRFP-C1	iRFP: MTOR$^{2021-2113}$:[GGSA]$_2$ QASNSAVDGTA:FIS1$^{122-152}$	This study
mCherry-FKBP-PI4KA^{C1001}	pmCherry-C1	mCherry: TagBFP2: FKBP1A$^{3-108}$:[GGSA]$_4$GG:PI4KA$^{1102-2103}$	(Zewe et al., 2020)

Table 1: plasmids. HUGO Gene names and protein numbering are indicated. Human sequences were used unless a species is indicated (except for fluorescent proteins).

All plasmids were validated across the open reading frame by dideoxy sequencing.

Cell Culture and Transfection

COS-7 cells (ATCC CRL-1651) were cultured in DMEM (5.56 mM glucose, glutaMAX supplement, Thermo Fisher 10567022) supplemented with 10% fetal bovine serum (ThermoFisher 10438-034), 10 u/ml penicillin and 10 µg/ml streptomycin (Thermofisher 15140122) and 1% (v/v) chemically defined lipid supplement (ThermoFisher 11905031). They were passaged twice weekly by rinsing in phosphate buffered saline and dissociation in Trypsin

like-enzyme (ThermoFisher 12604039) before diluting 1:5 into fresh media. For transfection, cells were plated in 35 mm petri dishes with 20 mm aperture #1.5 optical glass bottoms (CellVis D35-20-1.5-N) coated with 5 µg/ml fibronectin (ThermoFisher 33016-015) at 25-50% confluence. 1-24 h post seeding, cells were transfected by the addition of 200 µl of Opti-MEM (ThermoFisher 51985091) pre-complexed for > 20 min with 1 µg DNA and 3 µg lipofectamine 2000 (ThermoFisher 11668019); DNA and lipofectamine were each diluted to 100 µl before combining. Specific plasmid mixtures are indicated in the figures. Prior to imaging, media was replaced with 2 ml of complete HEPES imaging media, composed of FluoroBrite media (ThermoFisher A1896702) supplemented with 10% fetal bovine serum, 1% (v/v) chemically defined lipid supplement, 2 mM glutaMAX (ThermoFisher 35050061) and 25 mM Na-HEPES, pH 7.4.

Confocal Microscopy

A Nikon A1R-HD resonant scanning laser confocal microscope was used, mounted on a Nikon TiE inverted microscope stand. Images were collected through a 1.45 NA, plan apochromatic oil immersion objective (Nikon). Green (EGFP) and far red (iRFP713) fluorescence were co-excited using the 488 and 640 nm laser lines of a fiber-coupled LUN-V combiner, whereas red (mCherry) fluorescence was excited on a subsequent line scan to avoid cross talk, using the 561 nm laser line. Emission was collected using the following filters: green (505-550 nm), yellow-orange (570-620 nm) and far-red (650-850 nm). Confocal planes were collected with a pinhole of 1.2 Airy Units calculated for the far-red channel in resonant mode with 8 or 16 frame averaging. For time lapse imaging, up to 10 fields of cells were selected using the motorized stage, and imaged every 30 s. Addition of rapamycin was accomplished by pipetting 0.5 ml of complete HEPES imaging media containing 5 µM rapamycin (Fisher Scientific BP2963-1) to the 2 ml already in the dish, achieving a final bath concentration of 1 µM.

Total Internal Reflection Fluorescence Microscopy

A Nikon motorized TIRF illuminator mounted on a Nikon TiE inverted microscope stand was used. Laser excitation was fiber coupled from a four-line (405, 488, 561 and 638 nm) combiner (Oxxius). Emission was collected through dual pass filters from Chroma: blue/yellow-orange (420-480 nm / 570-620 nm) and green/far-red (505-550 nm / 650-850 nm). Imaging was performed through a 1.45 NA, plan apochromatic oil immersion objective (Nikon) using an Andor Zyla 5.5 sCMOS camera. For time-lapse imaging, up to 10 individual fields were marked

using the motorized stage and imaged every 30 s. 0.5 ml of 5 µM Rapamycin (Fisher Scientific BP2963-1) + 150 nM GSK-A1 (Sigma SML2453) were added after 2 min to achieve bath concentrations of 1 µM and 30 nM, respectively.

Quantitative Image Analysis and Statistics

For confocal image analysis, quantification of P4Mx2 signal at ER-PM or mitochondria-PM contact sites was accomplished by using the FRB-ER or mitochondria-FRB channels to generate a binary mask, and measuring the normalized intensity of P4Mx2 inside this mask compared to outside. This and the auto thresholding procedure used to generate these masks has been outlined in detail in a recent protocols paper (Wills et al., 2021). Briefly, the FRB images were Gaussian filtered at lengths defined by 1 and 2 multiples of the far red-fluor airy disc size (for ER), or 1, 2, 3 and 4 times this size for mitochondria. Each filtered image was subtracted from the image filtered at next smallest length scale to generate wavelet images. These wavelets were multiplied together and a threshold applied based on 0.5 standard deviations of the original image intensity, generating a binary mask. Finally, for mitochondria, the mask underwent a 2 pixel dilation to effectively cover all mitochondrial area in the image.

Analysis of TIRFM data was much simpler. After background subtraction, normalized intensity of the cell footprint was measured at each timepoint F_t, and normalized to the mean of the pre-stimulation intensity (F_{pre}).

Data analysis, statistics and graphs were plotted using Graphpad Prism 9. Details of statistical tests are given in the figure legends.

Acknowledgements

We are grateful to Jen Liou (UT SouthWestern, USA) for sharing EGFP-MAPPER. We are grateful to all members of the Hammond lab for technical assistance with experiments during restrictive COVID mitigation. This works was supported by NIH grant R35GM119412. All authors declare no competing financial interests.

References

Bojjireddy N, Botyanszki J, Hammond G, et al. (2014) Pharmacological and Genetic Targeting of the PI4KA Enzyme Reveals Its Important Role in Maintaining Plasma Membrane Phosphatidylinositol 4-Phosphate and Phosphatidylinositol 4,5-Bisphosphate Levels*. *Journal of Biological Chemistry* 289(9): 6120–6132. DOI: 10.1074/jbc.m113.531426.

Chang C-L, Hsieh T-S, Yang TT, et al. (2013) Feedback Regulation of Receptor-Induced Ca2+ Signaling Mediated by E-Syt1 and Nir2 at Endoplasmic Reticulum-Plasma Membrane Junctions. *Cell Reports* 5(3): 813–825. DOI: 10.1016/j.celrep.2013.09.038.

Cheong FY, Sharma V, Blagoveshchenskaya A, et al. (2010) Spatial Regulation of Golgi Phosphatidylinositol-4-Phosphate is Required for Enzyme Localization and Glycosylation Fidelity. *Traffic* 11(9): 1180–1190. DOI: 10.1111/j.1600-0854.2010.01092.x.

Chung J, Torta F, Masai K, et al. (2015) PI4P/phosphatidylserine countertransport at ORP5- and ORP8-mediated ER–plasma membrane contacts. *Science* 349(6246): 428–432. DOI: 10.1126/science.aab1370.

Eisenreichova A, Różycki B, Boura E, et al. (2021) Osh6 Revisited: Control of PS Transport by the Concerted Actions of PI4P and Sac1 Phosphatase. *Frontiers in Molecular Biosciences* 8: 747601. DOI: 10.3389/fmolb.2021.747601.

Filippin L, Abad MC, Gastaldello S, et al. (2005) Improved strategies for the delivery of GFP-based Ca2+ sensors into the mitochondrial matrix. *Cell Calcium* 37(2): 129–136. DOI: 10.1016/j.ceca.2004.08.002.

Filseck JM von, Čopič A, Delfosse V, et al. (2015) Phosphatidylserine transport by ORP/Osh proteins is driven by phosphatidylinositol 4-phosphate. *Science* 349(6246): 432–436. DOI: 10.1126/science.aab1346.

Hammond GRV, Machner MP and Balla T (2014) A novel probe for phosphatidylinositol 4-phosphate reveals multiple pools beyond the GolgiLocalization of PtdIns4P in living cells. *The Journal of Cell Biology* 205(1): 113–126. DOI: 10.1083/jcb.201312072.

Lipp N-F, Gautier R, Magdeleine M, et al. (2019) An electrostatic switching mechanism to control the lipid transfer activity of Osh6p. *Nature Communications* 10(1): 3926. DOI: 10.1038/s41467-019-11780-y.

McLaughlin S, Wang J, Gambhir A, et al. (2002) PIP2 AND PROTEINS: Interactions, Organization, and Information Flow. *Biophysics and Biomolecular Structure* 31(1): 151–175. DOI: 10.1146/annurev.biophys.31.082901.134259.

Mesmin B, Bigay J, Moser von Filseck J, et al. (2013) A Four-Step Cycle Driven by PI(4)P Hydrolysis Directs Sterol/PI(4)P Exchange by the ER-Golgi Tether OSBP. *Cell* 155(4): 830–843. DOI: 10.1016/j.cell.2013.09.056.

Prinz WA, Toulmay A and Balla T (2020) The functional universe of membrane contact sites. *Nature Reviews Molecular Cell Biology* 21(1): 7–24. DOI: 10.1038/s41580-019-0180-9.

Saint-Jean M de, Delfosse V, Douguet D, et al. (2011) Osh4p exchanges sterols for phosphatidylinositol 4-phosphate between lipid bilayers. *The Journal of Cell Biology* 195(6): 965–978. DOI: 10.1083/jcb.201104062.

Sengupta N, Jović M, Barnaeva E, et al. (2019) A large scale high-throughput screen identifies chemical inhibitors of phosphatidylinositol 4-kinase type II alpha[S]. *Journal of Lipid Research* 60(3): 683–693. DOI: 10.1194/jlr.d090159.

Sohn M, Korzeniowski M, Zewe JP, et al. (2018) PI(4,5)P2 controls plasma membrane PI4P and PS levels via ORP5/8 recruitment to ER–PM contact sitesRegulation of PM PI(4,5)P2 levels via ORP5/8. *The Journal of Cell Biology* 217(5): 1797–1813. DOI: 10.1083/jcb.201710095.

Stojanovski D, Koutsopoulos OS, Okamoto K, et al. (2004) Levels of human Fis1 at the mitochondrial outer membrane regulate mitochondrial morphology. *Journal of Cell Science* 117(7): 1201–1210. DOI: 10.1242/jcs.01058.

Tóth B, Balla A, Ma H, et al. (2006) Phosphatidylinositol 4-Kinase IIIβ Regulates the Transport of Ceramide between the Endoplasmic Reticulum and Golgi*. *Journal of Biological Chemistry* 281(47): 36369–36377. DOI: 10.1074/jbc.m604935200.

Wang Y, Mousley CJ, Lete MG, et al. (2019) An equal opportunity collaboration between lipid metabolism and proteins in the control of membrane trafficking in the trans-Golgi and endosomal systems. *Current Opinion in Cell Biology* 59: 58–72. DOI: 10.1016/j.ceb.2019.03.012.

Wills RC, Pacheco J and Hammond GRV (2021) Phosphoinositides, Methods and Protocols. *Methods in Molecular Biology* 2251: 55–72. DOI: 10.1007/978-1-0716-1142-5_4.

Wong LH, Gatta AT and Levine TP (2019) Lipid transfer proteins: the lipid commute via shuttles, bridges and tubes. *Nature Reviews Molecular Cell Biology* 20(2): 85–101. DOI: 10.1038/s41580-018-0071-5.

Zewe JP, Wills RC, Sangappa S, et al. (2018) SAC1 degrades its lipid substrate PtdIns4P in the endoplasmic reticulum to maintain a steep chemical gradient with donor membranes. *eLife* 7: e35588. DOI: 10.7554/elife.35588.

Zewe JP, Miller AM, Sangappa S, et al. (2020) Probing the subcellular distribution of phosphatidylinositol reveals a surprising lack at the plasma membrane. *Journal of Cell Biology* 219(3). DOI: 10.1083/jcb.201906127.

Figures

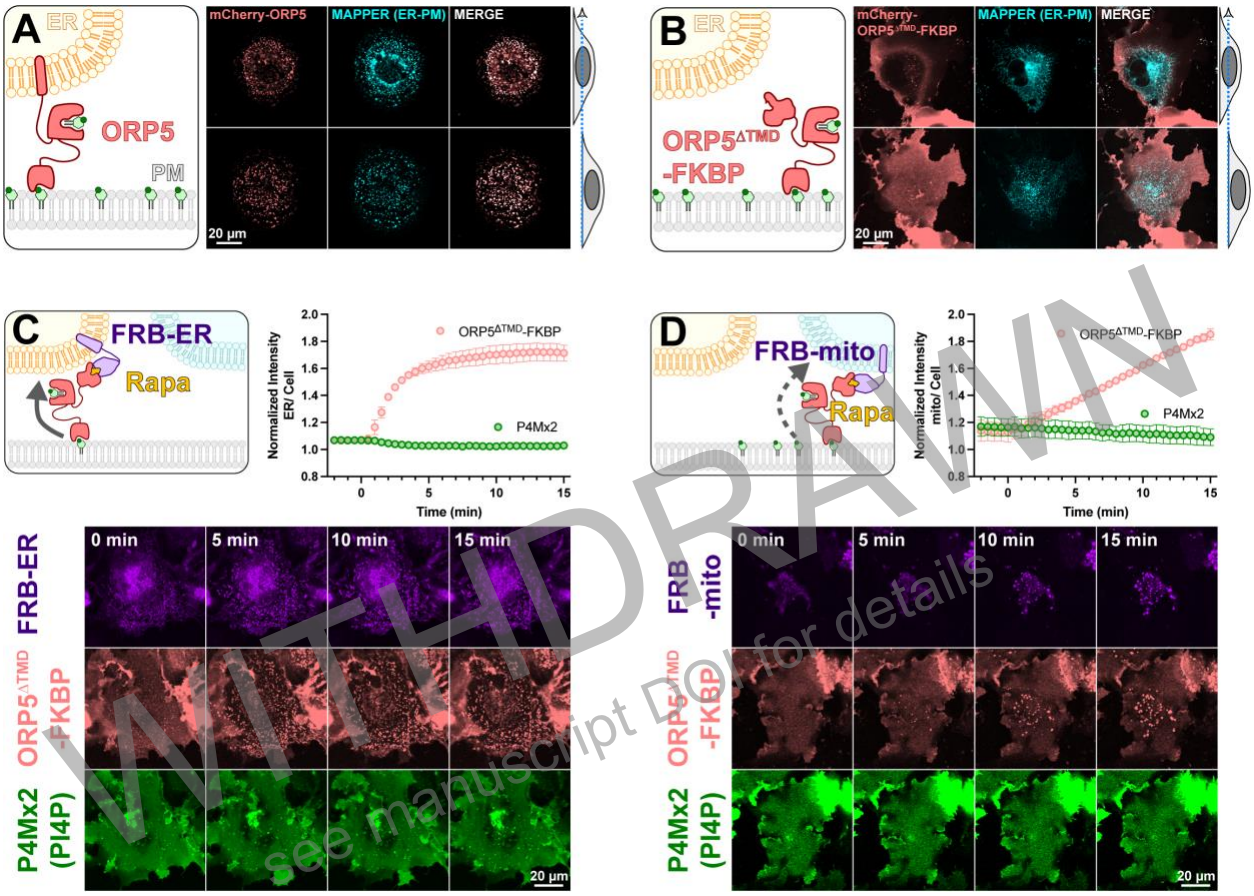

Figure 1: An engineered ORP5 ectopically targeted to PM-mitochondria contact sites fails to transfer PI4P. (**A**) mCherry-ORP5 localizes to ER-PM contact sites marked by the ER-PM contact site marker, MAPPER. Images show equatorial and ventral confocal sections of the same, representative cells. (**B**) Replacement of the ER-resident transmembrane domain (TMD) of ORP5 with FKBP leads to a de-localized PM localization, overlapping with MAPPER-labelled ER-PM contact sites, but not restricted to them. (**C**) mCherry-ORP5$^{\Delta TMD}$-FKBP can be returned to ER-PM contact sites by rapamycin-induced dimerization with an ER-localized FRB domain (iRFP-FRB-ER) though no enrichment of PI4P is seen at these induced contact sites. (**D**) mCherry-ORP5$^{\Delta TMD}$-FKBP can be targeted to ectopic mitochondria-PM contact sites by rapamycin-induced dimerization with an mitochondria-localized FRB domain (AKAP1^{N31}-FRB-iRFP), though again no enrichment of PI4P is seen at these induced contact sites. For **C & D**, images show ventral confocal sections of representative cells; the graphs show the normalized mCherry-ORP5$^{\Delta TMD}$-FKBP or P4Mx2 PI4P biosensor enrichment at ER or mitochondria contact sites, respectively. Data are grand means ± s.e. of three experiments, with 10 cells per experiment.

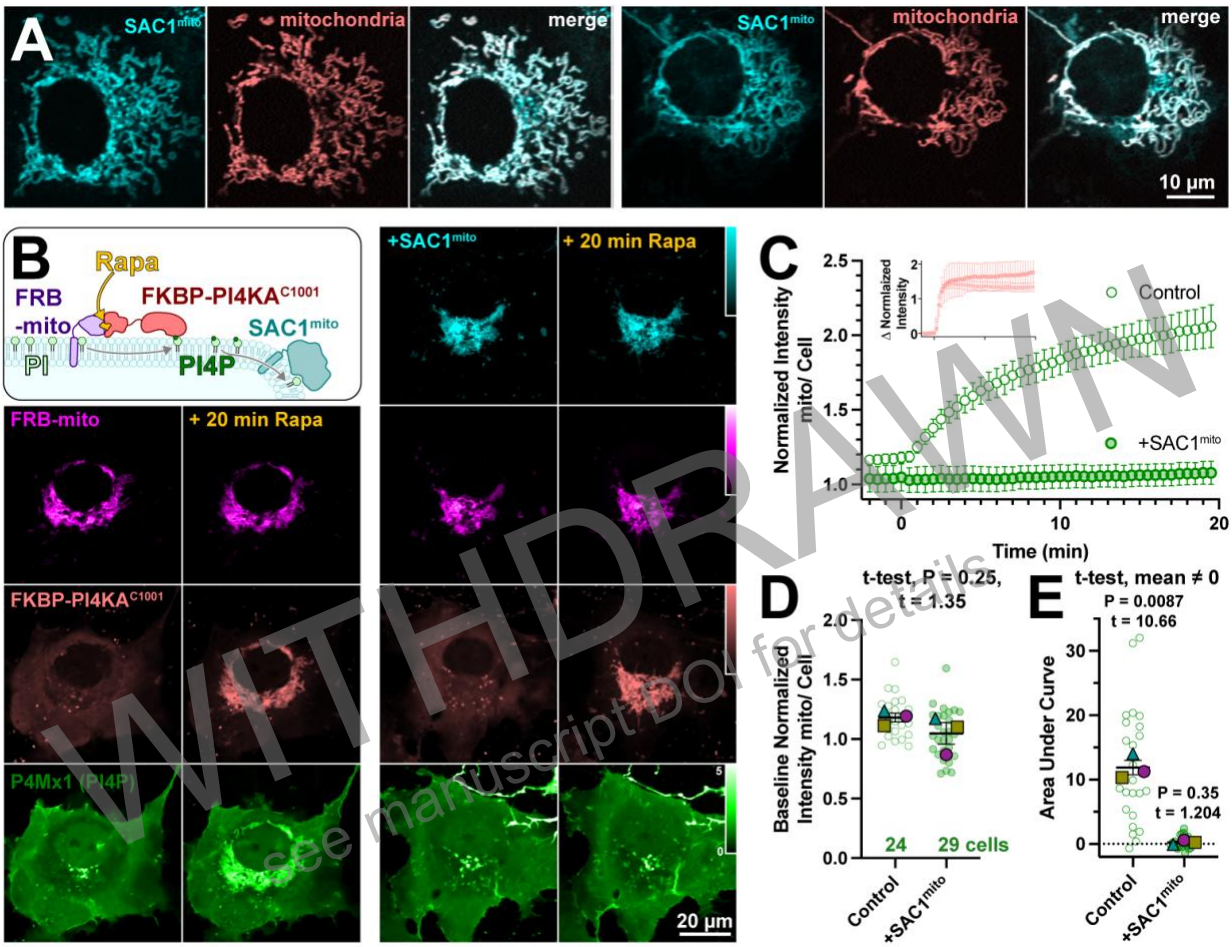

Figure 2: An engineered mitochondria-targeted SAC1 is active in cells. (**A**) SAC1^{mito} co-localizes with the mitochondrial marker, COX8A^{N29}x2-mCherry (pink). Images show representative equatorial confocal sections of two COS-7 cells. (**B**) Mitochondrial PI4P synthesis was induced by addition of rapamycin, which induces dimerization of over-expressed mCherry-FKBP-PI4K^{C1001} with iRFP-FRB-mito; this initiates ectopic PI4P synthesis on mitochondria outer membranes, detected with EGFP-P4Mx1 biosensor. The accumulation is blocked by co-expression of tagBFP2-SAC1^{mito}. Images show equatorial confocal sections of COS-7 cells before or after addition of rapamycin. P4Mx1 intensity is normalized to the average cell intensity, as quantified in B. (**C**) PI4P accumulation on mitochondria is blocked by SAC1^{mito}, despite equally efficient PI4KA^{C1001} recruitment (inset). (**D**) The slightly decreased baseline level of PI4P at mitochondria is not statistically significant by nested t-test. Smaller green points show individual cells (7-11 cells/experiment) and larger colored shapes show means of each of 3 experiments. Grand means ± s.e.m. are also indicated. (**E**) Complete reduction of mitochondrial PI4P synthesis, demonstrated by a grand mean of the area under the curve for SAC1^{mito}-expressing cells of 0.24 ± 0.20, not significantly different from 0 by t-test.

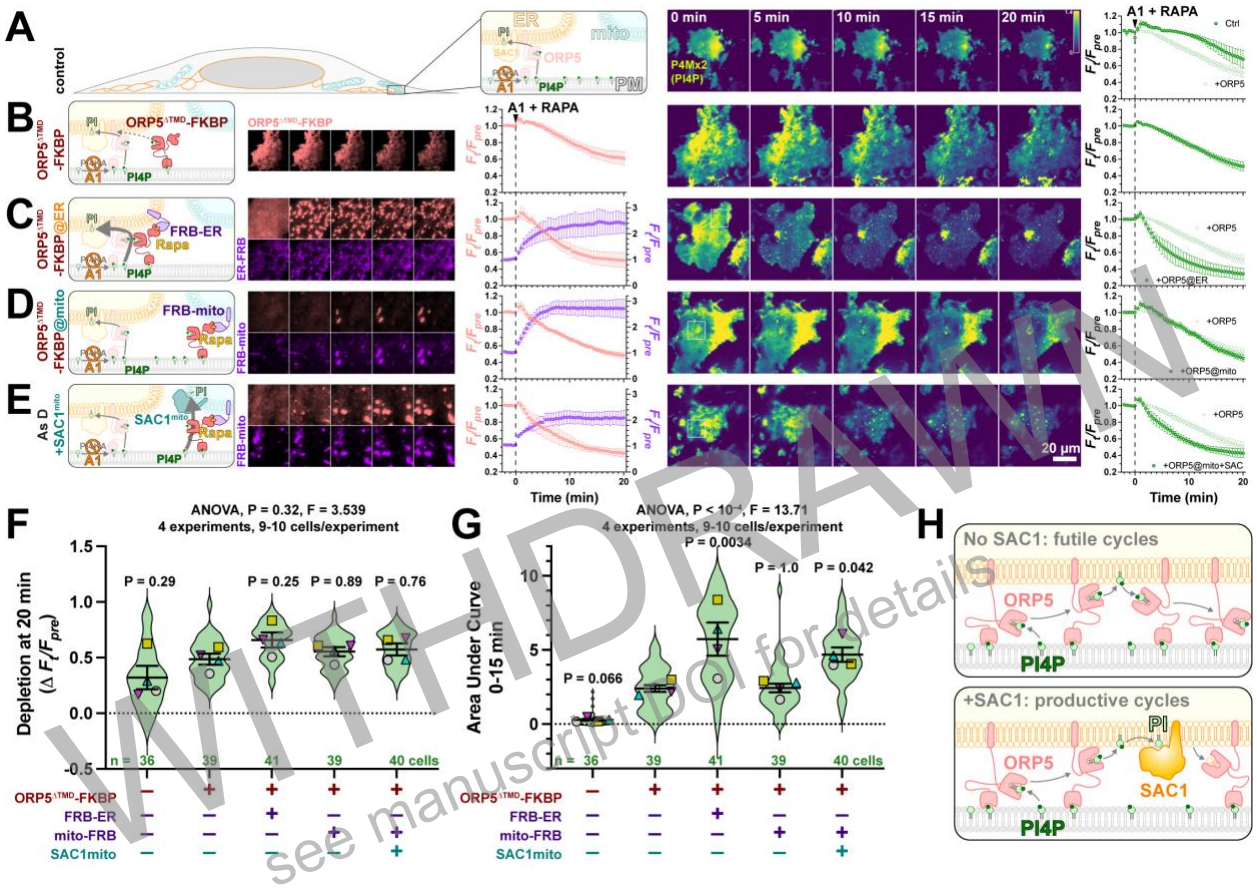

Figure 3: PI4P hydrolysis is required for productive inter-organelle PI4P transfer cycles (**A-E**) PI4P levels in COS-7 cells were measured with TIRFM using EGFP-P4Mx2 biosensors. At time 0, 1 μm rapamycin was applied to induce dimerization of any expressed FRB and FKBP proteins, along with 30 nM GSK-A1 to stop PM PI4P synthesis by PI4KA. PI4P turnover is then assessed over 20 mins. Graphs at right of images show the quantification of fluorescence intensity from color-matched channels to the left. 15 μm insets are displayed for FRB and FKBP where indicated on the PI4P images of whole cells. (**A**) In control cells, PI4P depletion is expected to occur due to transfer of PI4P to ER-localized SAC1 by endogenous ORP5, among other mechanisms. (**B**) over-expression of mCherry-ORP5$^{\Delta TMD}$-FKBP may slightly accelerate depletion, whereas recruitment of the protein using an ER-localized FRB (iRFP713-FRB-SAC1^{TMD}, **C**) causes greatly accelerated PM PI4P depletion. On the other hand, recruitment of mCherry-ORP5$^{\Delta TMD}$-FKBP to mitochondrial outer membrane localized FRB (iRFP713-FRB-Fis1^{C31}, **D**) does not accelerate PI4P depletion, unless it is co-expressed with a mitochondrial outer membrane-localized SAC1 (SAC1^{mito}, **E**). Graphs show means ± s.e. of the grand means of four experiments. Statistical analysis is presented for the total extent of depletion of PI4P at 20 mins in **F** or the rate of depletion (assessed as area under the curve during the first 15 mins) in **G**. Violin plots show the distribution of values from all cells measured across all four experiments; overlaid points show means of each experiment, and line and error bars show grand mean ± s.e. The results of a one-way nested-ANOVA are indicated, with Dunnet's post-hoc analysis comparing all values to mCherry-ORP5$^{\Delta TMD}$-FKBP alone. (**H**) Model for how SAC1 prevents futile cycles due to high-affinity binding of ORP5 ORD to PI4P.